Li, C.; Vidal Moya, JA.; Miguel, PJ.; Dedecek, J.; Boronat Zaragoza, M.; Corma Canós, A. (2018). Selective Introduction of Acid Sites in Different Confined Positions in ZSM-5 and Its Catalytic Implications. ACS Catalysis. 8(8):7688-7697. https://doi.org/10.1021/acscatal.8b02112

Selectively Introducing Acid Sites in Different Confined Positions in ZSM-5 and its Catalytic Implications

Chengeng Li,[†] Alejandro Vidal-Moya,[†] Pablo J. Miguel,[§] Jiri Dedecek,[‡] Mercedes Boronat[†,*] and Avelino Corma[†,*]

[†]Instituto de Tecnología Química, Universitat Politècnica de València, Consejo Superior de Investigaciones Cientificas, Av. de los Naranjos, s/n, 46022 Valencia, Spain

[§]Departamento de Ingeniería Química, Universitat de València, Av. de la Universitat, s/n, 46100 Burjassot, Spain

[‡]J. Heyrovsky Institute of Physical Chemistry, Academy of Sciences of the Czech Republic, Dolejskova 3, CZ-182 23 Prague 8, Czech Republic

Supporting Information

ABSTRACT: Controlling the location of acid sites in zeolites can have a great impact on catalysis. In this work we face the objective of directing the location of Al into the 10R channels of ZSM-5 by taking advantage of the structural preference of B to occupy certain positions at the channels intersections, as suggested by theoretical calculations. The synthesis of B-Al-ZSM-5 zeolites with variable Si/Al and Si/B ratio, followed by B removal in a post synthesis treatment, produces ZSM-5 samples enriched in Al occupying positions at 10R channels. The location of the acid sites is determined on the basis of the product distribution of 1-hexene cracking as test reaction. The higher selectivity to propene and lower $C_4^=/C_3^=$ ratio in the samples synthesized with B and subsequently deboronated can be related to a larger concentration of acid sites in 10R channels, where monomolecular cracking occurs. Finally, several ZSM-5 samples have been tested in the methanol to propene reaction, and those synthesized through the B assisted method show longer catalytic lifetime, higher propene yield and lower yield of alkanes and aromatics.

KEYWORDS: Zeolites, DFT, Al-siting, Boron ZSM-5, MTO, catalytic cracking.

INTRODUCTION

Controlling the location of acid sites in zeolites can have a great impact on their catalytic behavior. The Brönsted acidity in zeolites is associated to protons compensating the negative charge generated by the presence of framework Al in tetrahedral T sites. The complexity of the crystal structure in zeolite frameworks generates multiple topologically distinguishable T sites that, when occupied by Al, originate Brönsted acid sites with the protons facing different cavities or channels. The intrinsic acid strength of Brönsted sites associated to Al located at different T positions is similar when described rigorously by deprotonation energies (DPE), [1-5] but their catalytic behavior in terms of activity and selectivity can differ with the location, due to the influence of confinement effects on intermediates and transition states.[6-10]

A paradigmatic case in where the control of the acid site distribu tion can have important practical implications is the MFI framework, whose aluminosilicate form is the medium pore ZSM-5 zeolite. The channel system of MFI is composed by interconnected straight (10R-str) and sinusoidal (10R-sin) ten-membered ring channels of ~ 5.0 Å diameter, that intersect forming larger void spaces of ~ 7.0 Å diameter (see Figure 1). The Brönsted acid sites resulting from isomorphic substitution of Al by Si in ZSM-5 can point towards the channels or towards the open space generated at the channels intersection depending on Al location. Despite the fact that both types of acid sites can interact with a given reactant molecule, the molecular confinement and therefore the enthalpic and entropic effects on the adsorbed reactant and on the transition state in the two environments will not be necessarily the same.[7-13]

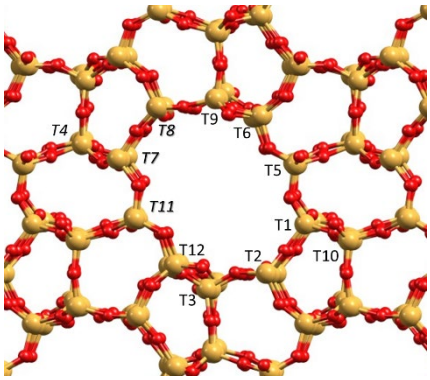

Figure 1. Crystallographic T positions in MFI framework.

ZSM-5 is one of the two zeolites used in the industrial transformation of methanol to olefines (MTO), the other one being SAPO-34 with the CHA structure. The MTO process is an efficient way to obtain light olefins, such as ethene and propene, by successive methylation and cracking of the so-called hydrocarbon pool (HP) organic intermediates that act as co-catalysts of the reaction.[14-16] The detailed reaction mechanism, product distribution and catalyst deactivation are closely related to the zeolite topology and pore architecture. In the larger channels and cavities of BEA and CHA catalysts, polymethylbenzenes (PMB) are the main HP species, and the side-chain route generating both ethene and propene is the most probable pathway. In MFI, a dual-cycle mechanism has been proposed, according to which ethene is formed via the aromatics-based HP mechanism while propene and higher alkenes are formed

through methylation/cracking of C_3^+ alkene intermediates.[14,15,17-19] The suppression of the aromatics-based cycle in H-ZSM-22 zeolite containing an unidirectional system of non-intersecting straight 10R channels[20] suggests that, in H-ZSM-5, the polymethylbenzene HP species are formed in the channels intersections, while the alkene-based cycle is active within the 10R channels. Therefore, it is inferred that the propene/ethene selectivity in the MTO process, as well as the amount of aromatics and alkanes resulting from bimolecular hydrogen transfer processes preferentially occuring at the channels intersections, could be modified by controlling the location of the Brönsted acid sites within the MFI framework.

Researchers have attempted to tune acid site location in FER,[21,22] CHA,[23,24] RTH[25] and MFI[26-32] zeolite frameworks by developing new synthetic strategies that combine different aluminium or silicon sources, organic structure directing agents (OSDAs) and inorganic compensating cations. Despite changes in catalytic performance associated to the synthetic route employed have been reported several times, only in some cases the origin of the catalytic diversity could be identified, and related either to the presence of Al at particular cavities or channels[21,22] or to its nature as isolated or paired Al centres.[24] The unambiguous identification of the Al siting in the 12 distinct T sites of H-ZSM-5 zeolite is particularly challenging, and has been attempted by means of ^{27}Al-MAS-NMR, UV-Vis of Co^{2+}, chemical adsorption and catalytic experiments.[26-32] Deconvolution of the ^{27}Al-MAS-NMR spectra of ZSM-5 into different peaks has allowed to demonstrate that Al siting in this zeolite varies with the synthesis conditions, and that several different T sites are occupied by Al even in samples with high Si/Al ratio.[33-35] However, while different deconvolution patterns are indicative of a different Al distribution within the MFI framework, a clear assignation of the peaks to particular positions is not established yet. Another aspect considered in relation to Al distibution is the proximity between Al atoms, and their local arrangement as isolated, paired - defined as framework Al atoms separated by either one or two Si atoms [Al-O(-Si-O)$_x$-Al, x=1,2]- or unpaired species, which are separated by more than three Si atoms but are close enough to compesate the charge of a divalent cation. The concentration of Al in each of the three arrangements can be estimated by combining Co^{2+} and Na^+ ion-exchanging capacity, and the characterization of the paired species as α, β and γ can be determined by deconvolution of the diffuse reflectance UV-Vis spectra of dehydrated Co^{2+} exchanged samples.[26,27,30,36]

Another strategy to control the Al distribution within a given zeolite framework is based on isomorphous substitution with a second trivalent heteroatom, usually boron, that might preferentially compete with Al for some T sites. The succesful regulation of the Al siting through competitive incorporation of B has been recently achieved in H-MCM-22 zeolite. The preferential location of B in T positions facing the surface pockets and supercages of the MWW structure, prone to carbonaceous depositions, concentrates the Brönsted acid sites associated to Al into the 10R sinusoidal channels, where the alkene-based cycle is sterically favored. As a consequence, the modified catalyst exhibits a high selectivity to propene and butenes, and an improved long-term stability.[37,38]

There are some examples in the literature reporting an enhanced stability against deactivation by coke formation in B-modified ZSM-5 catalysts, which has been attributed to an increase in the amount of weak acid sites associated to B.[39-42] However, no clear trends in the propene/ethene selectivity have been observed, and no direct relationship between B or Al siting and catalytic performance has been established.

In this work we use the competitive Al and B incorporation in the ZSM-5 framework as starting working hypothesis to preferentially locate Al atoms and the associated Brönsted acid sites in the 10R channels of ZSM-5, with the final objective of increasing the selectivity to propene, reducing the amount of aromatics and alkanes, and improving the catalyst stability.

To achieve this goal, we have first studied by Density Functional Theory (DFT) the preferred location, if there is any, of Al and B in the MFI structure. Then, Al-B-ZSM-5 zeolites with different Si/Al and Si/B ratios have been synthesized and characterized, and in a second step B has been selectively removed by post synthesis treatments. To determine the relative population of Brönsted acid sites associated to the remaining Al in the 10R channels or at the channels intersections we have used the product selectivity obtained in a test reaction, 1-hexene cracking, that undergoes different mono- and bimolecular reactions depending on the space available around the active sites. Comparison with the results obtained using a unidimensional 10R pore zeolite (Theta-1) leads to the conclusion that the method proposed allows to modify the relative amount of Al atoms, and consequently of acid sites, within the channels versus channels intersections, and that it is possible to prepare, on those bases, improved catalysts for the conversion of methanol to propene.

RESULTS AND DISCUSSION

DFT study of Al and B location in ZSM-5

The hypothesis that B and Al tend to occupy different T positions in ZSM-5 was investigated by means of DFT calculations (see Computational Details in the Supporting Information). Among the twelve non-equivalent tetrahedral T sites present in the orthorrombic structure of ZSM-5, T4 and T10 are located in the sinusoidal 10R-sin channel, T8 and T11 are in the straight 10R-str channel, and the rest (T1, T2, T3, T5, T6, T7, T9 and T12) are at the intersection between the 10R-sin and 10R-str channels. Previous quantum chemical calculations agree that the difference in energy between the most and least stable location of Al is not larger than 9 kcal/mol.[11,43,44] In a first step, six different systems with chemical composition $Al_xSi_{96-x}O_{192}$ and $B_xSi_{96-x}O_{192}$, with x = 1, 2 and 4 were generated to model ZSM-5 zeolite with different Si/Al and Si/B ratios, and twelve different distributions corresponding to placing the Al or B atoms in the same crystallographic T position, from T1 to T12, were considered for each chemical composition. The negative charge generated in the framework by the presence of Al an B was compensated by tetraethyl ammonium cations in a tg.tg conformation occluded at the channels intersections.[45] The relative stabilities of all distributions with respect to the most stable one are summarized in Table 1.

Table 1. Relative stability of Al and B distributions (in kcal/mol) of Al-ZSM-5 and B-ZSM-5 zeolite models with different Si/Al and Si/B ratios.

	Si/Al			Si/B		
	95	47	23	95	47	23
T1	0.0	1.2	1.6	3.4	3.0	9.0
T2	3.1	6.4	2.6	4.9	9.3	7.4
T3	2.6	5.7	0.4	6.4	11.4	13.2
T4	1.4	0.6	2.8	5.9	7.8	22.5
T5	1.7	0.9	5.4	0.7	0.0	6.7
T6	4.0	8.0	6.4	2.1	2.1	0.0
T7	3.3	8.3	16.3	3.4	6.6	17.4
T8	1.9	3.6	4.6	5.4	9.5	22.0
T9	3.1	5.8	5.3	3.5	6.1	6.1
T10	1.5	4.5	5.4	0.0	0.5	2.2
T11	1.3	0.0	0.9	1.9	1.4	7.8
T12	0.1	0.1	0.0	3.5	5.1	8.6

In agreement with previous studies,[11,43,44] the energy values obtained for the Al-containing models are quite similar, within 4 kcal/mol at high Si/Al ratio and within 8 kcal/mol at most at higher Al content, with the only exception of T7 position that is clearly unstable at Si/Al = 23 (see Table 1 and Figures 2 and S1). This result is in accordance with the proposal that Al siting in ZSM-5 depends on the synthesis procedure,[33-35] because there is not any

clear thermodynamic preference for occupying any given position in the framework. Indeed, at the highest Al content considered, there are six different positions whose relative stability differs by less than 3 kcal/mol: T1, T2, T3 and T12 at the channels intersections and T4 and T11 within the 10R channels. In contrast, in the B-containing models, differences in stability larger than 6 kcal/mol are already obtained at high Si/B ratio, that significantly increase with the B content. Thus, only T5, T6, T10 and T11 are within 3 kcal/mol at low and medium B content. Increasing the Si/B ratio to 23 results in a clear destabilization of most distributions, and the results in Table 1 and Figures 2 and S1 indicate that B atoms exhibit a clear thermodynamic preference to occupy T6 position at the channels intersection followed by T10 in the sinusoidal 10R-sin channel. This preferential siting of B at T6 and T10 is maintained in mixed Al-B-ZSM-5 models in which two Al and two B atoms are placed at the same T position (see Table 2).

Table 2. Relative stability of Al and B distributions (in kcal/mol) of Al-B-ZSM-5 zeolite models with Si/(Al+B) = 23 and Al/B = 1.

Al	B	E_{rel}	Al	B	E_{rel}	Al	B	E_{rel}
T1	T1	3.6	T4	T5	5.3	T11	T6	3.2
T2	T2	6.5	T4	T6	1.7	T11	T10	4.6
T3	T3	6.8	T4	T10	1.9	T12	T5	5.9
T4	T4	8.7	T4	T11	7.9	T12	T6	1.2
T5	T5	5.1	T5	T6	10.5	T12	T10	3.3
T6	T6	3.6	T5	T10	4.8	T12	T11	7.3
T7	T7	15.9	T5	T11	7.2	T6	T4	16.2
T8	T8	13.8	T8	T5	10.7	T6	T5	11.9
T9	T9	7.5	T8	T6	1.4	T6	T8	13.3
T10	T10	3.2	T8	T10	7.9	T6	T10	3.6
T11	T11	7.0	T8	T11	9.0	T6	T11	8.2
T12	T12	8.4	T10	T5	9.7	T6	T12	9.8
T1	T5	5.5	T10	T6	9.5	T2	T6	0.0
T1	T6	7.2	T10	T11	8.5	T3	T6	3.2
T1	T10	1.3	T10	T4	11.9	T7	T6	10.7
T1	T11	4.1	T11	T5	9.5	T9	T6	3.8

To try to understand the origin of the higher stability of B substitution at certain T positions, some geometrical parameters like the average Si-Si bond length in the pure silica material or the distance between the T atom and the N atom of the quaternary ammonium cation are summarized in Table S1 together with the relative stability of each Al and B distribution at high Si/Al and Si/B ratios. While no clear trend is observed for Al distribution, the plot in Figure S2 suggests that B is more stable at those T sites with shorter Si-Si distances, in line with the smaller size of the BO_4 unit as compared to AlO_4.

Then, other possible distributions of Al and B in which the two heteroatoms occupy different T positions were explored, with B being preferentially placed at T5, T6, T10 and T11 due to the significant differences in stability obtained for substitution of this heteroatom and the large computational effort required to include all possibilities. Data in Table 2 confirm the trend that the most stable systems (within ~ 4 kcal/mol) contain B in either T6 or T10, irrespectively of the location of Al. Indeed, exchanging the Al and B positions in the most stable configurations always led to a significant destabilization of the system, as for instance T4-T6, T4-T10, or T6-T8 (see Table 2). It should also be noticed that three out of the six most stable distributions, whose relative energy differs by less than 3 kcal/mol, correspond to Al siting at T4, T8 and T11, that is, within the 10R channels (see Table 2 and Figure 2). Comparison of the plots in Figure 2a and 2c suggests that the presence of B increases the proportion of stable configurations containing Al in the 10R channels. It can then be concluded from the DFT calculations that, from a thermodynamic point of view, Al has little tendency to occupy preferentially any of the 12 T positions in ZSM-5 zeolite, in agreement with previous reports.[11,43,44] On the other hand, B prefers to occupy T6 and T10 sites at or close to the channels intersection rather than any other position and, consequently, the proportion of T sites within the channels occupied by Al increases.

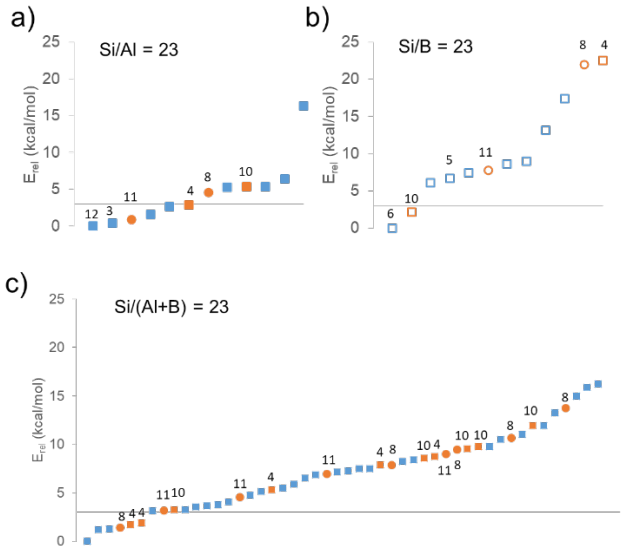

Figure 2. Relative energy (in kcal/mol) with respect to the most stable distribution in a) Al-ZSM5 with Si/Al=23, b) B-ZSM5 with Si/B=23, and c) Al-B-ZSM-5 with Si/(Al+B)=23 and Al/B=1.Full and open symbols indicate location of Al and B, respectively. T sites at channels intersections are plotted in blue, orange squares and circles correspond to T sites within the 10R-sin and 10R-str channels, respectively. Some T sites are indicated by numbers.

Synthesis and Characterization of Al-B-ZSM-5 zeolites

It can therefore be envisioned that, by synthesizing Al-B-ZSM-5 zeolites with a Si/(Al+B) ratio of ~ 23 and Al/B ratio of ~ 1, and selectively removing the B with post-synthesis treatments, we could obtain Al-ZSM-5 samples with a higher proportion of Al in the channels than in the case of conventionally prepared Al-ZSM-5 zeolite. To confirm this hypothesis, Al-ZSM-5 and B-ZSM-5 samples with different Si/Al and Si/B ratios, as well as the corresponding Al-B-ZSM-5 samples with different B/Al ratios were prepared (Table 3). The Si/(Al+B) ratio in the B-containing gels ranged from 11.5 to 33.3. Notice that the T_{total}/OSDA ratios (Table 4) in one unit cell in all the as-synthesized samples were calculated to be near 24, based on the results of elemental analysis. This is, as well, the amount of available positive charges for T^{III} heteroatoms to be located, limiting the minimum Si/(Al+B) in the resultant product to be 24. As a result, the cases with Si/(Al+B) lower than 24 should force competitive incorporation of Al and B in the available sites. Data in Table 3 indicate that, in these cases (samples labelled -B2), all Al present in the synthesis gel is incorporated into the zeolite framework while only a fraction of the B initially present in the gel is finally located in the zeolite structure.

Crystallinity, chemical analysis and textural properties of the Si-Al, Si-B and Si-Al-B ZSM-5 zeolites before and after deboronation are given in Figure 3 and Table 4. The XRD patterns of all synthesized ZSM-5 samples showed the characteristic diffraction peaks of the MFI topology (Figure 3A). After the deboronation and calcination process the samples preserved the crystallinity (Figure 3B), indicating that the removal of most of the B (Table 4) does not cause notable destruction of the framework structure. This conclusion is supported by the observation that the micropore volume of the zeolite samples remains practically the same after the deboronation treatment. It is also important to notice that no changes in the Al content of the Si-Al-B samples was observed due to the above postsynthesis treatments (Table 3).

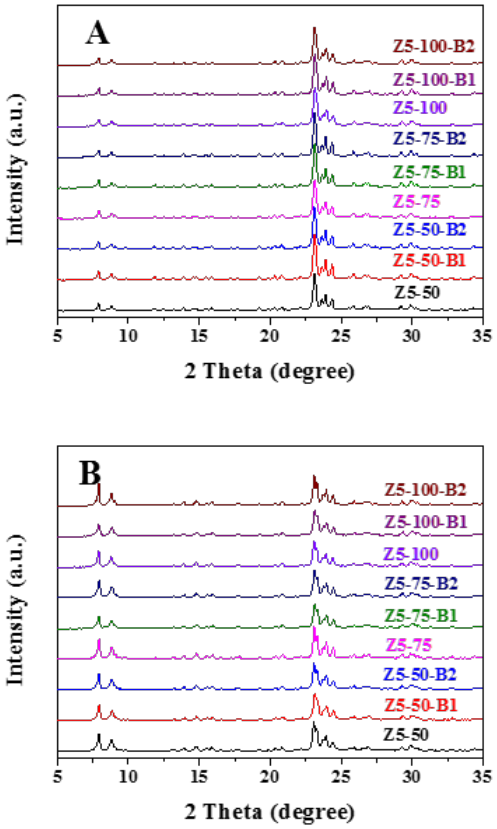

Figure 3. XRD patterns of ZSM-5 samples in as-synthesized forms (A) and after deboronation process (B).

Table 3. Chemical composition of different ZSM-5 samples.

Sample	Composition gel[a]			As-synthesized[a]			Deboronated[b]	
	Si/Al	Si/B	Si/(Al+B)	Si/Al	Si/B	Si/(Al+B)	Si/Al	Si/B
Z5-pureB	-	50	50	-	45	45	-	107
Z5-50	50	-	50	43	-	43	44	-
Z5-50-B1	50	50	25	44	49	23.2	46	82
Z5-50-B2	50	15	11.5	47	49	24.0	48	96
Z5-75	75	-	75	58	-	58	58	-
Z5-75-B1	75	50	30	60	67	31.7	61	117
Z5-75-B2	75	15	12.5	72	40	25.7	70	64
Z5-100	100	-	100	86	-	86	86	-
Z5-100-B1	100	50	33.3	87	77	40.8	90	149
Z5-100-B2	100	15	13.0	90	39	27.2	92	78

[a] measured by ICP-AES
[b] measured by elemental analysis

Table 4. Characterization of different ZSM-5 samples.

Sample	OSDA (wt%)[a]	T_{total}/ OSDA	S_{BET} (m^2/g)	V_{micro} (cm^3/g)	S_{ext} (m^2/g)
Z5-pureB	11.79	23.2	382	0.17	47
Z5-50	11.47	24.0	401	0.17	53
Z5-50-B1	11.28	24.4	364	0.17	49
Z5-50-B2	11.34	24.3	400	0.16	83
Z5-75	11.57	23.7	378	0.16	41
Z5-75-B1	11.14	24.8	391	0.17	61
Z5-75-B2	11.62	23.6	395	0.17	44
Z5-100	11.45	24.0	375	0.16	43
Z5-100-B1	11.31	24.4	390	0.17	38
Z5-100-B2	11.78	23.3	388	0.17	41

[a] measured by elemental analysis

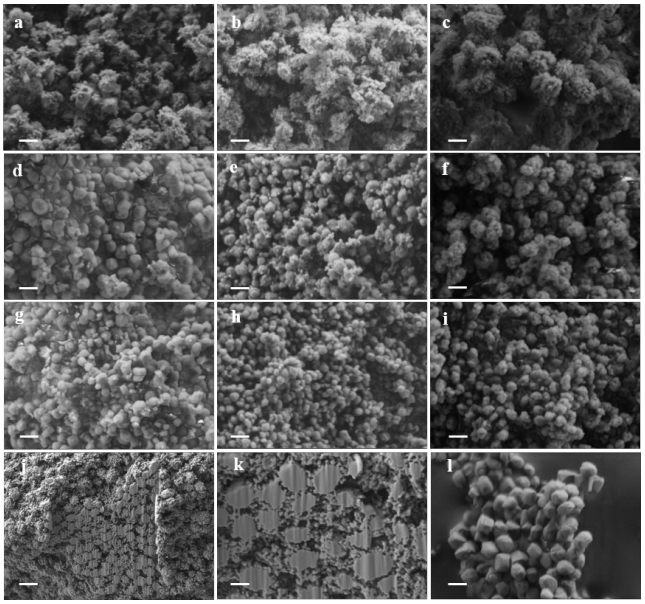

Figure 4. SEM images of ZSM-5 samples (a) Z5-50 (b) Z5-50-B1 (c) Z5-50-B2 (d) Z5-75 (e) Z5-75-B1 (f) Z5-75-B2 (g) Z5-100 (h) Z5-100-B1 (i) Z5-100-B2 (j, k) Z5-50-B1 (l) Z5-pureB. The scale bar in the images represents a length of 200 nm.

Another key parameter to define and compare catalytic activity of different zeolite samples is the crystallite size, which has been measured here by FESEM. The results obtained (Figure 4) indicate that all ZSM-5 samples, regardless of their framework composition, are formed by nanosized crystals of 100-200 nm. Moreover, samples with medium and high Si/Al ratios (Z5-75 (Figure 4d-f) and Z5-100 series (Figure 4g-i)) have spherical morphology with clean external surface. Samples of the Z5-50 series with relatively higher Al content show also the presence of smaller crystallites (Figure 4a-c). The internal sections of the samples analyzed by FIB-SEM (Figure 4j, k) illustrate that, despite some aggregation of the nanoparticles occur, the crystals were well defined with sizes between 100 and 200 nm, being the pattern very similar for all the samples. Therefore we will be able to compare the catalytic activity of the samples on the bases of their framework composition and the way of achieving this composition for a constant zeolite crystallite size. The acid properties of the deboronated ZSM-5 samples were characterized by NH_3-TPD and FT-IR combined with pyridine adsorption/desorption measurements (see Figure S3, S4 and Table S2 in the Supporting Information). The total amount of acid sites correlates with the Si/Al ratio of the samples, and the absence of pyridine adsorption in a pure B-ZSM-5 zeolite prepared for comparison purposes confirms that residual B does not significantly contributes to the measured acidity after removal of B.

^{27}Al MAS NMR spectra (Figure 5) show the presence of an intense peak at ~ 55 ppm assigned to tetrahedrally coordinated Al in all samples, while the band corresponding to extraframework Al at ~ 0 ppm was not observed in any case. In order to obtain information about the Al distribution in each sample, the broad signal ranging from 45 to 65 ppm was deconvoluted into five different peaks at 52, 53, 54, 56 and 58 ppm (see the ^{27}Al 3QMAS NMR spectrum of the Z5-50 and Z5-50-B samples in Figure S5) following the procedure previously described by Yokoi et al.[28] The curve fittings and relative peak areas of the ^{27}Al MAS NMR spectra of the different ZSM-5 samples are given in Figure 6 and Table 5. The relative concentration of the five peaks differs noticeably from one sample to another, with the only exception of the two samples with higher Si/Al ratio, Z5-100 and Z5-100-B1, which are quite similar. However, there is not a clear trend regarding the changes in intensity associated to the presence

of B in Z5-50 and Z5-75 series. It can therefore be concluded that there is a different distribution of Al atoms over the 12 non-equivalent tetrahedral T sites present in ZSM-5 in the samples with low Si/Al ratio caused by the competitive introduction of B in the framework, an effect that is not observed at high Si/Al ratio. However, it is not possible at this point to assign the peaks to particular T positions and therefore to identify the location of Al based only on ^{27}Al MAS NMR spectra.

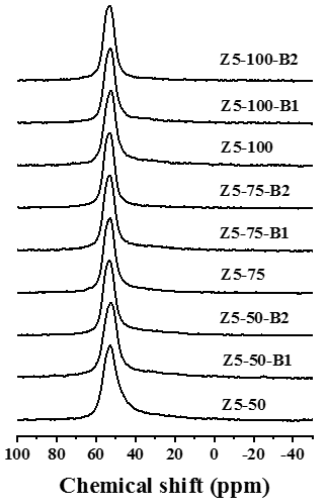

Figure 5. ^{27}Al MAS NMR spectra of different ZSM-5 samples.

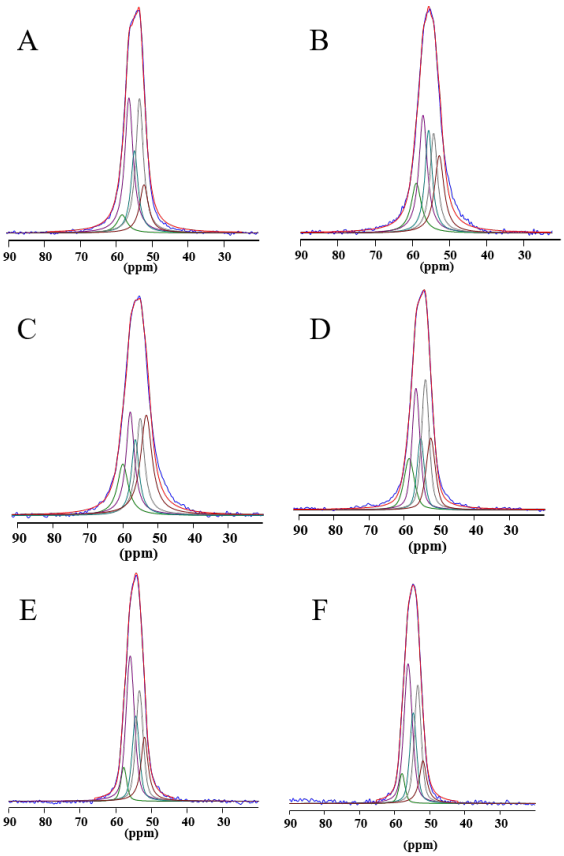

Figure 6. Curve fitting of the ^{27}Al MAS NMR spectra of (A) Z5-50, (B) Z5-50-B1, (C) Z5-75, (D) Z5-75-B1 (E) Z5-100 and (F) Z5-100-B1.

Table 5. Relative peak areas of the ^{27}Al MAS NMR spectra of different ZSM -5 samples.

	Al(e)	Al(d)	Al(c)	Al(b)	Al(a)
chemical shift (ppm)	58	56	54	53	52
Z5-50	6	33	18	30	13
Z5-50-B1	13	26	20	20	21
Z5-75	14	22	15	21	28
Z5-75-B1	12	30	13	28	17
Z5-100	6	36	19	24	15
Z5-100-B1	5	36	20	26	12

Table 6. Co^{2+}-exchange experiment results of different ZSM-5 samples.

Sample	Composition[a]		Co-exchange experiment				
	Si/Al	Si/B	Al_{isol}[b]	Al_{pair}[c]	Al_{α}[d]	Al_{β}[d]	Al_{γ}[d]
Z5-50	44	-	45%	55%	32%	65%	3%
Z5-50-B1	46	82	30%	70%	45%	55%	<1%

[a]Measured by ICP-AES
[b]Calculated according to equation $n(Al_{isol})=n(Al_{total})-n(Al_{pair})$
[c]$n(Al_{pair})= n(Co^{2+})$
[d]Measured by deconvolution of UV-Vis spectra of dehydrated ZSM-5.

Finally, the concentration of isolated and paired Al atoms in samples Z5-50 and Z5-50-B1, and the characterization of the paired species as α, β and γ was determined by means of Co^{2+} and Na^{+} ion-exchange experiments and by deconvolution of the diffuse reflectance UV-Vis spectra of dehydrated Co^{2+} exchanged samples, following the procedures described in the literature.[26,27,30,31,46] The results summarized in Table 6 indicate that the percentage of paired Al sites is higher in Z5-50-B1 sample, probably because the presence of B in the framework forces Al atoms to become closer. As regards the relative concentration of the different types of Al pairs present in the two samples, namely α (at the straight channels), β (at the intersections) and γ (at the sinusoidal channels), the trend observed is that the relative amount of Al sites in the straight 10R channels associated to α–pairs is higher in sample Z5-50-B1, although nothing can be stated about the location of the isolated Al atoms.

The characterization work described above shows that, after removal of B from the initially synthesized Si-Al-B-ZSM-5 zeolites, we have samples with similar crystal size, Si/Al ratio and acid properties as the corresponding Si-Al-ZSM-5 prepared by conventional procedures, but with a different distribution of Al within the framework. Therefore, the final activity and selectivity should be directly related to framework Al and its location within the structure. To determine the relative concentration of active sites in channels and intersections we use a test reaction, 1-hexene cracking, as a characterization tool. We are aware that a test reaction is an indirect proof subjected to interpretation, but at the same time it can give indications about whether the reactant is able to interact with sites with different molecular constrains and reactivity.

Cracking of 1-hexene as a test reaction for site location

Cracking of olefins can proceed through mono- or bimolecular processes, and the tendency to go through either process depends mainly on the size of the substrate molecule. Olefins with less than six carbons preferentially follow a bimolecular cracking pathway, and larger olefins generally favor the monomolecular route. We have selected 1-hexene cracking as test reaction because this molecule is on the boundary, that is, it can crack through both mono- and bimolecular processes and therefore, in this particular case, the

ability of the zeolite framework to confine and stablilize the intermediates and transition states involved in each pathway becomes particularly relevant.

According to the mechanistic scheme for 1-hexene cracking (Scheme 1), the monomolecular pathway can either occur through branching isomerization of linear hexyl carbenium ions followed by β-scission yielding propene, or via direct β-scission of hexyl cations producing linear butenes and ethene, this latter possibility being less favorable because it requires the formation of secondary-primary carbenium ions. The bimolecular pathway involves the reaction of 1-hexene with propyl cations generated via the monomolecular route to form bulkier C_9^+ carbenium ions that subsequently crack into different size olefins ($C_2^=$ - $C_6^=$). It can be expected that formation of such bulky cationic intermediates, as well as other accompanying bimolecular reactions like oligomerization, cyclization and hydrogen transfer yielding aromatics and alkanes, will only occur at the channels intersections, while the monomolecular pathway will also be allowed to occur on sites located within the 10R channels. Thus, the selectivity parameters associated to these reactions should provide information about the location of the active sites.

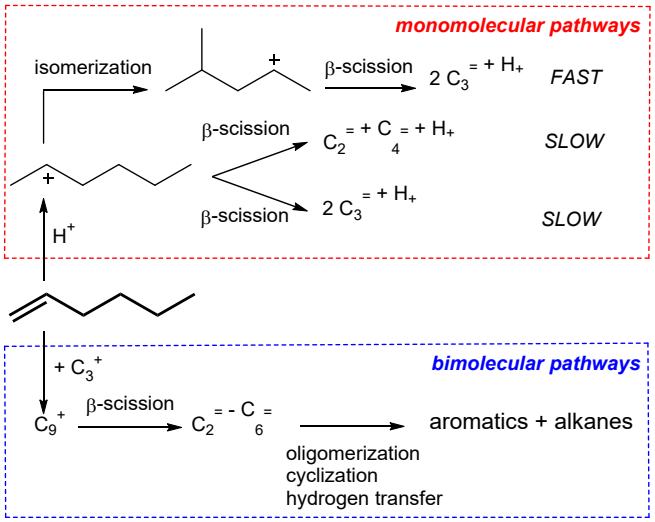

Scheme 1. Pathways for mono- and bimolecular cracking of 1-hexene in ZSM-5.

Table 7 summarizes the product distribution of 1-hexene cracking on Z5-50 and Z5-50-B1 samples at 500 ºC, atmospheric pressure, and an intermediate feed partial pressure (x_o=0.251) (see Catalytic Reactions Section in the Supporting Information), together with results previously obtained using a unidimensional 10R zeolite such as Theta-1 with similar Si/Al ratio.[47] The main products obtained are propene, butenes, pentenes and ethene, followed by small amounts of alkanes and aromatics. It is important to remark that the mono- and bimolecular processes cannot be distinguished directly from the product distribution since the olefins, which are the main products, could be both products and reactants of several primary and secondary reactions. However, following the reaction scheme, it is reasonable to assume that the monomolecular cracking of 1-hexene mainly follows the isomerization-β-scission route yielding propene. This is supported by the low yield of ethene obtained in all cases, and specially with the unidimensional Theta-1 sample in where bimolecular processes are practically forbidden. On the other hand, if the $C_4^=$ observed was only formed by monomolecular cracking of 1-hexene, then the $C_2^=/C_4^=$ ratio should be equal to one. However, the results in Table 7 and Figure S6 show that such ratio is lower than one in the three samples, although larger in Theta-1 than in ZSM-5, and therefore it can be concluded that a large fraction of the $C_4^=$ detected is formed by bimolecular cracking. If this

Table 7. Conversion and product distribution of 1-hexene cracking on Z5-50, Z5-50-B1 and Theta-1.

Sample		Z5-50	Z5-50-B1	Theta-1
Contact time (s)		9.96	14.94	39.8
Conversion (%)		84.3	84.7	82.9
Molar yield (%)	Ethene	13.3	12.9	8.5
	Propene	78.3	86.2	122.1
	$C_4^=$	33.8	30.9	13.9
	$C_5^=$	12.6	11.8	4.4
	$C_7^=$	0.4	0.3	0.3
Molar yield ratio	$C_2^=/C_4^=$	0.39	0.42	0.61
	$C_4^=/C_3^=$	0.43	0.36	0.11
	$C_5^=/C_3^=$	0.16	0.14	0.04

is so, it appears that the $C_4^=/C_3^=$ ratio could be used on a comparative basis to discuss the relative extension of bimolecular with respect to monomolecular cracking in the different samples prepared. Results in Table 7 and Figure S6 clearly show that the $C_4^=/C_3^=$ ratio is lower in the Z5-50-B1 sample, synthesized with B and then removed, than in the Z5-50 zeolite, and much lower in the unidirectional Theta-1. A similar trend, although less pronounced, is found for the $C_5^=/C_3^=$ ratio. These results suggest a higher ratio of mono- versus bimolecular cracking in the ZSM-5 sample originally synthesized with B and ulteriorly removed, which in turn may indicate that this material has a larger fraction of Al active sites located within the 10R channels, in agreement with the DFT and Co^{2+}-exchange results.

This conclusion would also agree with the experimental fact that the selectivity for accompanying reactions that involve bimolecular processes and lead to formation of alkanes are lower with the sample synthesized with B and then removed (see Table S3 in the Supporting Information), which is expected to have a larger fraction of acid sites within the channels. Taking into account the small size of the crystallites and the fact that these bimolecular processes can also occur at the external surface of the catalysts, the influence of the external acid sites was investigated by conducting the catalytic cracking of 1-hexene in the presence of a poisoning agent, 2,4-dimethylquinoline (2,4-DMQ), that selectively blocks the acid sites on the external surface. The initial conversion of 1-hexene decreases by ~5-10% due to the presence of 2,4-DMQ, especially on Z5-50 sample, indicating that the reaction mainly occurs inside the channels, and the influence of the external surface is small (see Figure S7 in the Supporting Information). As regards selectivity, data in Table S3 show that the presence of 2,4-DMQ mainly affects the bimolecular processes, but still the ratio of mono- versus bimolecular cracking is larger for the Z5-50-B1 sample.

In conclusion, by means of 1-hexene cracking as a test reaction we have seen that in two ZSM-5 samples with similar Si/Al ratio, crystal size, micropore volume and same external surface area, the sample synthesized with B that is later removed by a post synthesis treatment (Z5-50-B1) gives a higher ratio of mono- to bimolecular cracking than the sample that was synthesized without B (Z5-50), which could be interpreted because the proportion of cracking occuring within the channels is higher in the former catalyst. If this is so, it appears to us that the catalytic behavior of the Z5-50-B1 sample should approach more to that of a unidimensional 10R zeolite such as Theta-1 (see Table 7 and Figure 7). This similarity should however take into account diffusion limitations in the unidirectional Theta-1 zeolite that would lead to a lower rate of reaction as compared to Z5-50-B1 sample, in where the active sites in the 10R channels are accessible from the channel intersection void volume. This is indeed confirmed by the results presented in Figure 7, that includes reaction data of Theta-1 with Si/Al = 44 in the catalytic

cracking of 1-hexene taken from a previously published work.[47] Furthermore, if the "dimensionality" of the Theta-1 is increased by creating mesopores that reduce channel length and increase the number of accessible pore mouth sites, the cracking reaction rate of this modified Theta-1 zeolite approaches that of Z5-50-B1 sample.

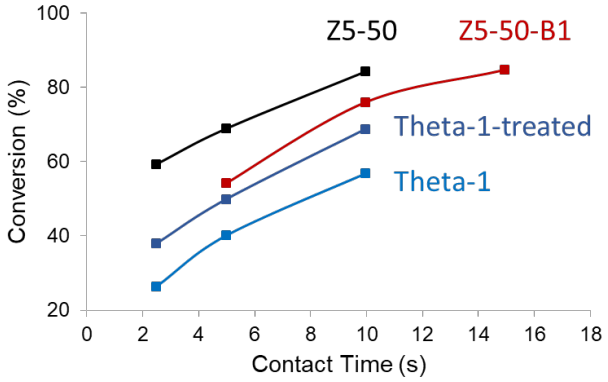

Figure 7. Initial Conversion of 1-hexene vs. contact time in 1-hexene cracking on Z5-50 (black), Z5-50-B1 (red) and Theta-1 (blue) samples.

It appears that, on the basis of the theoretical calculations and the results obtained with the test reaction, the hypothesis that B preferentially occupies framework positions at the channels intersection when competing with Al is a plausible one. Therefore, on those bases we should be able to design a better catalyst for other processes in where the location of Al in the ZSM-5 framework can be relevant for the selectivity of the reaction. For showing that, we have selected here the conversion of methanol to propene. This is an industrially relevant process, in where the olefins formed initially can keep reacting through bimolecular processes to give aromatics and alkanes. There is no doubt that the concept and catalysts we have presented above should have a positive impact on the selectivity to propene when feeding methanol.

Methanol to propene

The objective during the preparation of catalysts for converting methanol into propene with ZSM-5 is to synthesize samples that maximize the selectivity to propene while minimizing the extent of secondary oligomerization–cyclization–hydrogen transfer reactions yielding aromatics and alkanes. In this sense, it has been generally accepted that the density of acid sites, given by the framework Si/Al ratio, is the main compositional parameter that controls the extent of those secondary reactions, being the selectivity to aromatics and alkanes higher when the framework Si/Al ratio is lower. While this gives a good macroscopic picture on catalyst-reactivity, it is clear that if one goes deeper it is possible to predict that the Al content in the zeolite taken as a global number does not guarantee the Al distribution in the form of isolated or paired Al, neither the Al location in more or less constrained positions within the structure, unless ZSM-5 samples with very high Si/Al ratios are considered.

When the reaction mechanism for methanol conversion to olefins has been studied on ZSM-5, it has been found that $C_3^=$-$C_5^=$ olefins are initially formed and then, aromatics and alkanes start to appear while the olefins show an unstable behavior, indicating that they further react to give the aromatics.[48] According to the dual-cycle mechanism proposed in the literature, [14,15,17-19] propene and higher alkenes are formed through methylation/cracking of C_3^+ alkene intermediates preferentially within the 10R channels, while aromatics and alkanes resulting from oligomerization, cyclization and hydrogen transfer processes should occur at the channels intersections. If this is true, we should see a much higher selectivity to shorter chain olefins and much lower formation of aromatics and alkanes when carrying out the reaction with a unidimensional 10R zeolite. The same Theta-1 sample used in the catalytic cracking of 1-hexene was tested in the methanol to propene reaction and, indeed, the main products obtained were $C_3^=$-$C_5^=$ olefins, with very low amount of aromatics and alkanes (see Figure 8).[49,50]

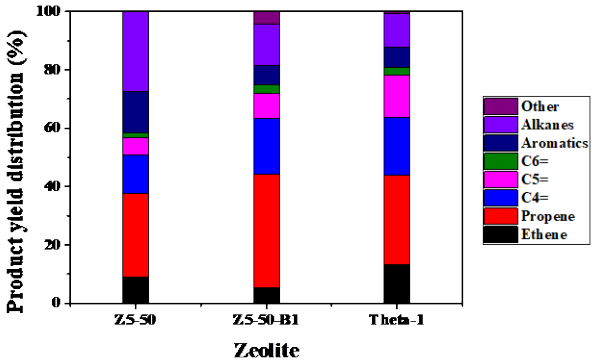

Figure 8. Product yield distribution of methanol to propene over different zeolites.

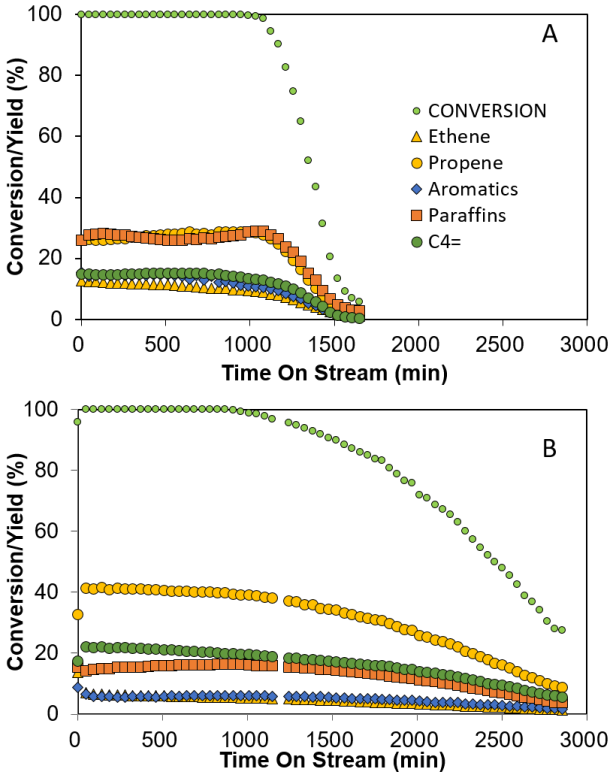

Figure 9. Product distribution of methanol to propene over (A) Z5-50 and (B) Z5-50-B1 samples. VHSW = 10 h^{-1}.

In order to obtain a similar product distribution using ZSM-5, the number of acid sites located within the 10R channels should be maximized, while those at the channels intersections should be kept to a minimum in order ot avoid the formation of aromatics with the corresponding loss of selectivity to propene and increase in catalyst deactivation. Taking into account all these considerations, it is clear that an approximation to the catalyst design can come from the Si-Al-B catalyst concept described above. Indeed, the results obtained with Z5-50 and Z5-50-B1 samples (see Catalytic Reactions Section

in the Supporting Information) show that the latter is more selective to propene and less selective to aromatics and alkanes, and that catalytic lifetime is significantly increased (see Figures 9 and S8). Results obtained with zeolites with different Si/Al ratios indicate that the introduction of B in the synthesis and ulterior removal has always a positive effect, but its relevance decreases when increasing the Si/Al ratios (Figure S8).

CONCLUSIONS

In conclusion, we have showed the relevance on catalytic activity, selectivity and catalyst decay of selectively locating the acid sites in positions with different confinement within the zeolite. This has been illustrated in the case of ZSM-5 by taking advantage of the different structural preference of B and Al to occupy positions within the 10R channels or at channels intersections. B is preferentially located at the channels intersections, while Al has no clear preference for any particular T site. Then, by preparing B-Al-ZSM-5 samples followed by B removal in a post synthesis treatment, it is possible to produce Al-ZSM-5 samples enriched with Al in the 10R channels. The effect of that has been illustrated for improving the selectivity to propene in 1-hexene cracking and methanol to propene reactions.

ASSOCIATED CONTENT

Supporting Information

Experimental details. Relative energy for ZSM-5 with various Si/Al and Si/B ratios, average Si-Si distances and their correlation with the relative energy. Acidity characterizations, ^{27}Al 3QMAS NMR of ZSM-5 samples with and without B. Product molar yield ratios as a function of conversion for different samples. 1-hexene cracking in presence of 2,4-DMQ as poisoning agent. MTO reaction results of ZSM-5 samples with various Si/Al and Si/B ratios.

AUTHOR INFORMATION

Corresponding Author

Avelino Corma, acorma@itq.upv.es

Mercedes Boronat, boronat@itq.upv.es

ORCID

Chengeng Li: 0000-0003-2004-5081

Pablo J. Miguel: 0000-0002-6706-8152

Jiri Dedecek: 0000-0002-3697-8815

Mercedes Boronat: 0000-0002-6211-5888

Avelino Corma: 0000-0002-2232-3527

Notes

The authors declare no competing financial interest.

ACKNOWLEDGMENT

This work was supported by the European Union through ERC-AdG-2014-671093 (SynCatMatch), the Spanish Government-MINECO through ‘‘Severo Ochoa” (SEV-2016-0683) and CTQ2015-70126-R. The Electron Microscopy Service of the UPV is acknowledged for their help in sample characterization. Red Española de Supercomputación (RES) and Centre de Càlcul de la Universitat de Valencia are gratefully acknowledged for computational resources and technical support. Li acknowledges China Scholarship Council (CSC) for a Ph.D fellowship.

REFERENCES

(1) Brand, H. V.; Curtiss, L. A.; Iton, L. E. Ab Initio Molecular Orbital Cluster Studies of the Zeolite ZSM-5. 1. Proton Affinities. *J. Phys. Chem.* **1993**, *97*, 12773–12782.

(2) Kassab, E.; Seiti, K.; Allavena, M. Determination of Structure and Acidity Scales in Zeolite Systems by Ab Initio and Pseudopotential Calculations. *J. Phys. Chem.* **1988***, 92,* 6705–6709.

(3) Brändle, M.; Sauer, J. Acidity Differences Between Inorganic Solids Induced by their Framework Structure. A Combined Quantum Mechanics/Molecular Mechanics Ab Initio Study on Zeolites. *J. Am. Chem. Soc.* **1998**, *120*, 1556 – 1570.

(4) Jones, A. J.; Carr, R. T. , Zones, S. I.; Iglesia, E. Acid Strength and Solvation in Catalysis by MFI Zeolites and Effects of the Identity, Concentration and Location of Framework Heteroatoms. *J. Catal.* **2014**, *312*, 58–68.

(5) Jones, A. J.; Iglesia, E. *ACS Catal.* The Strength of Brønsted Acid Sites in Microporous Aluminosilicates. **2015**, *5*, 5741 – 5755.

(6) Derouane, E. G. Zeolites as Solid Solvents 1. *J. Mol. Catal. A: Chem.* **1998**, *134*, 29 – 45.

(7) Knott, B. C.; Nimlos, C. T.; Robichaud, D. J.; Nimlos, M. R.; Kim, S.; Gounder, R. Consideration of the Aluminum Distribution in Zeolites in Theoretical and Experimental Catalysis Research. *ACS Catal.* **2018**, *8*, 770 – 784.

(8) Gounder, R.; Iglesia, E. The Catalytic Diversity of Zeolites: Confinement and Solvation Effects within Voids of Molecular Dimensions. *Chem. Commun.* **2013**, *49*, 3491 – 3509.

(9) Jones, A. J.; Iglesia, E. Kinetic, Spectroscopic, and Theoretical Assessment of Associative and Dissociative Methanol Dehydration Routes in Zeolites. *Angew. Chem. Int. Ed.* **2014**, 53, 12177 – 12181.

(10) Wang, S.; Iglesia, E. Catalytic Diversity Conferred by Confinement of Protons within Porous Aluminosilicates in Prins Condensation Reactions. *J. Catal.* **2017**, *352*, 415 – 435.

(11) Ghorbanpour, A.; Rimer, J. D.; Grabow, L. C. Periodic, vdW-Corrected Density Functional Theory Investigation of the Effect of Al siting in H-ZSM-5 on Chemisorption Properties and Site-Specific Acidity. *Catal. Commun.* **2014**, *52*, 98 – 102.

(12) Sharada, S. M.; Zimmerman, P. M.; Bell, A. T.; Head-Gordon, M. Insights into the Kinetics of Cracking and Dehydrogenation Reactions of Light Alkanes in H-MFI. *J. Phys. Chem. C* **2013**, *117*, 12600 – 12611.

(13) Janda, A.; Bell, A. T. Effects of Si/Al ratio on the Distribution of Framework Al and on the Rates of Alkane Monomolecular Cracking and Dehydrogenation in H-MFI. *J. Am. Chem. Soc.* **2013**, *135*, 19193 – 19207.

(14) Olsbye, U.; Svelle, S.; Bjørgen, M.; Beato, P.; Janssens, T. V. W.; Joensen, F.; Bordiga, S.; Lillerud, K. P. Conversion of Methanol to Hydrocarbons: How Zeolite Cavity and Pore Size Controls Product Selectivity. *Angew. Chem. Int. Ed.* **2012**, *51*, 5810 – 5831.

(15) Van Speybroeck, V.; De Wispelaere, K.; Van der Mynsbrugge, J.; Vandichel, M.; Hemelsoet, K.; Waroquier, M. First Principle Chemical Kinetics in Zeolites: the Methanol-to-Olefin Process as a Case Study. *Chem. Soc. Rev.* **2014**, *43*, 7326 – 7357.

(16) Tian, P.; Wei, Y.; Ye, M.; Liu, Z., Methanol to olefins (MTO): from fundamentals to commercialization. *ACS Catal.* **2015**, *5*, 1922 – 1938.

(17) Svelle, S.; Joensen, F.; Nerlov, J.; Olsbye, U.; Lillerud, K. P.; Kolboe, S.; Bjorgen, M. Conversion of Methanol into Hydrocarbons over Zeolite H-ZSM-5: Ethene Formation is Mechanistically Separated from the Formation of Higher Alkenes. *J. Am. Chem. Soc.* **2006**, *128*, 14770 – 14771.

(18) Bjorgen, M.; Svelle, S.; Joensen, F.; Nerlov, J.; Kolboe, S.; Bonino, F.; Palumbo, L.; Bordiga, S.; Olsbye, U. Conversion of Methanol to Hydrocarbons over Zeolite H-ZSM-5: On the Origin of the Olefinic Species. *J. Catal.* **2007**, *249*, 195– 207.

(19) Wang, S.; Chen, Y.; Wei, Z.; Qin, Z.; Ma, H.; Dong, M.; Li, J.; Fan, W.; Wang, J. Polymethylbenzene or Alkene Cycle? Theoretical Study on Their Contribution to the Process of Methanol to

Olefins over H-ZSM-5 Zeolite. *J. Phys. Chem. C* **2015**, *119*, 28482 – 28498.
(20) Teketel, S.; Olsbye, U.; Lillerud, K.P.; Beato, P.; Svelle, S. Selectivity Control Through Fundamental Mechanistic Insight in the Conversion of Methanol to Hydrocarbons over Zeolites. *Microporous Mesoporous Mater.* **2010**, *136*, 33– 41.
(21) Pinar, A. B.; Marquez-Alvarez, C.; Grande-Casas, M.; Perez-Pariente, J. Template-Controlled Acidity and Catalytic Activity of Ferrierite Crystals. *J. Catal.* **2009**, *263*, 258– 265.
(22) Román-Leshkov, Y.; Moliner, M.; Davis, M. E. Impact of Controlling the Site Distribution of Al Atoms on Catalytic Properties in Ferrierite-type Zeolites. *J. Phys. Chem. C* **2011**, *115*, 1096 – 1102.
(23) Di Iorio, J. R.; Gounder, R. Controlling the Isolation and Pairing of Aluminum in Chabazite Zeolites Using Mixtures of Organic and Inorganic Structure-Directing Agents. *Chem. Mater.* **2016**, *28*, 2236–2247.
(24) Di Iorio, J. R.; Nimlos, C. T.; Gounder, R. Introducing Catalytic Diversity into Single-Site Chabazite Zeolites of Fixed Composition via Synthetic Control of Active Site Proximity. *ACS Catal.* **2017**, *7*, 6663−6674.
(25) Liu, M.; Yokoi, T.; Yoshioka, M.; Imai, H.; Kondoa, J. N.; Tatsumi, T. Differences in Al Distribution and Acidic Properties between RTH-type Zeolites Synthesized with OSDAs and without OSDAs. *Phys.Chem.Chem.Phys.* **2014**, *16*, 4155– 4164.
(26) Dědeček, J.; Balgová, V.; Pashkova, V.; Klein, P.; Wichterlová, B. Synthesis of ZSM-5 Zeolites with Defined Distribution of Al Atoms in the Framework and Multinuclear MAS NMR Analysis of the Control of Al Distribution. *Chem. Mater.* **2012**, *24*, 3231−3239.
(27) Pashkova, V.; Klein, P.; Dědeček, J.; Tokarova, V.; Wichterlová, B. Incorporation of Al at ZSM-5 Hydrothermal Synthesis. Tuning of Al Pairs in the Framework. *Microporous Mesoporous Mater.* **2015**, *202*, 138 − 146.
(28) Yokoi, T.; Mochizuki, H.; Namba, S.; Kondo, J. N.; Tatsumi, T. Control of the Al Distribution in the Framework of ZSM-5 Zeolite and its Evaluation by Solid-State NMR Technique and Catalytic Properties. *J. Phys. Chem. C* **2015**, *119*, 15303−15315.
(29) Liang, T.; Chen, J.; Qin, Z.; Li, J.; Wang, P.; Wang, S.; Wang, G.; Dong, M.; Fan, W.; Wang, J. Conversion of Methanol to Olefins over H-ZSM-5 Zeolite: Reaction Pathway is Related to the Framework Aluminum Siting. *ACS Catal.* **2016**, *6*, 7311−7325.
(30) Pashkova, V.; Sklenak, S.; Klein, P.; Urbanova, M.; Dědeček, J. Location of Framework Al Atoms in the Channels of ZSM‐5: Effect of the (Hydrothermal) Synthesis. *Chem. Eur. J.* **2016**, *22*, 3937 − 3941.
(31) Yokoi, T.; Mochizuki, H.; Biligetu, T.; Wang, Y.; Tatsumi, T. Unique Al Distribution in the MFI Framework and Its Impact on Catalytic Properties. *Chem. Lett.* **2017**, *46*, 798− 800.
(32) Biligetu, T.; Wang, Y.; Nishitoba, T.; Otomo, R.; Park, S.; Mochizuki H.; Kondo J. N.; Tatsumi, T.; Yokoi, T. Al Distribution and Catalytic Performance of ZSM-5 Zeolites Synthesized with various Alcohols. *J. Catal.* **2017**, *353*, 1–10.
(33) Han, O. H.; Kim, C. S.; Hong, S. B. Direct Evidence for the Nonrandom Nature of Al Substitution in Zeolite ZSM-5: An Investigation by ^{27}Al MAS and MQ MAS NMR. *Angew. Chem. Int. Ed.* **2002**, *41*, 469 − 472.
(34) Sklenak, S.; Dědeček, J.; Li, C.; Wichterlová, B.; Gabova, V.; Sierka, M.; Sauer, J. Aluminum Siting in Silicon‐Rich Zeolite Frameworks: A Combined High‐Resolution ^{27}Al NMR Spectroscopy and Quantum Mechanics/Molecular Mechanics Study of ZSM-5. *Angew. Chem. Int. Ed.* **2007**, *46*, 7286 − 7289.
(35) Sklenak, S.; Dědeček, J.; Li, C.; Wichterlová, B.; Gabova, V.; Sierka, M.; Sauer, J. Aluminium Siting in the ZSM-5 Framework by Combination of High Resolution ^{27}Al NMR and DFT/MM Calculations. *Phys. Chem. Chem. Phys.* **2009**, *11*, 1237 − 1247.
(36) Dědeček, J.; Sobalík, Z.;Wichterlová, B. Siting and Distribution of Framework Aluminium Atoms in Silicon-rich Zeolites and Impact on Catalysis. *Catalysis Reviews: Science and Engineering* **2012**, *54*, 135 − 223.
(37) Wang, S.; Wei, Z.; Chen, Y.; Qin, Z.; Ma, H.; Dong, M.; Fan, W.; Wang, J. Methanol to Olefins over H-MCM-22 Zeolite: Theoretical Study on the Catalytic Roles of various Pores. *ACS Catal.* **2015**, *5*, 1131 − 1144.
(38) Chen, J.; Liang, T.; Li, J.; Wang, S.; Qin, Z.; Wang, P.; Huang, L.; Fan, W.; Wang, J. Regulation of Framework Aluminum Siting and Acid Distribution in H-MCM-22 by Boron Incorporation and Its Effect on the Catalytic Performance in Methanol to Hydrocarbons. *ACS Catal.* **2016**, *6*, 2299 − 2313.
(39) Zhu, Q.; Kondo, J. N.; Yokoi, T.; Setoyama, T.; Yamaguchi, M.; Takewaki, T.; Domen, K.; Tatsumi, T. The Influence of Acidities of Boron- and Aluminium-containing MFI Zeolites on co-reaction of Methanol and Ethene. *Phys. Chem. Chem. Phys.* **2011**, *13*, 14598 − 14605.
(40) Yang, Y.; Sun, C.; Du, J.; Yue, Y.; Hua, W.; Zhang, C.; Shen, W.; Xu, H. The Synthesis of Endurable B–Al–ZSM-5 Catalysts with Tunable Acidity for Methanol to Propylene Reaction *Catal. Commun.* **2012**, *24*, 44 − 47.
(41) Hu, Z.; Zhang, H.; Wang, L.; Zhang, H.; Zhang, Y.; Xu, H.; Shen, W.; Tang, Y. Highly Stable Boron-Modified Hierarchical Nanocrystalline ZSM-5 Zeolite for the Methanol to Propylene Reaction. *Catal. Sci. Technol.* **2014**, *4*, 2891− 2895.
(42) Yaripour, F.; Shariatinia, Z.; Sahebdelfar, S.; Irandoukht, A. Effect of Boron Incorporation on the Structure, Products Selectivities and Lifetime of H-ZSM-5 Nanocatalyst Designed for Application in Methanol-to-Olefins (MTO) Reaction. *Microp. Mesop. Mater.* **2015**, *203*, 41 − 53.
(43) Nachtigallova, D.; Nachtigall, P.; Sierka, M.; Sauer, J. Coordination and Siting of Cu^+ ions in ZSM-5: A Combined Quantum Mechanics/Interatomic Potential Function Study. *Phys. Chem. Chem. Phys.* **1999**, *1*, 2019 − 2026.
(44) Schröder, K.P.; Sauer, J.; Leslie, M.; Catlow, C. R. A. Siting of Al and Bridging Hydroxyl Groups in ZSM-5: A Computer Simulation Study. *Zeolites* **1992**, *12*, 20 – 23.
(45) Schmidt, J. E.; Fu, D.; Deem, M. W.; Weckhuysen, B. M. Template‐Framework Interactions in Tetraethylammonium‐Directed Zeolite Synthesis. *Angew. Chem. Int. Ed.* **2016**, *55*, 16044 – 16048.
(46) Dedecek, J.; Kaucky, D.; Wichterlova, B.; Gonsiorova, O. Co^{2+} Ions as Probes of Al Distribution in the Framework of Zeolites. ZSM-5 study. *Phys. Chem. Chem. Phys.*, **2002**, *4*, 5406–5413.
(47) Blay, V.; Miguel, P. J.; Corma, A. Theta-1 Zeolite Catalyst for Increasing the Yield of Propene when Cracking Olefins and its Potential Integration with an Olefin Metathesis Unit. *Catal. Sci. Technol.* **2017**, *7*, 5847-5859.
(48) Sun, X.; Mueller, S.; Shi, H.; Haller, G.; Sanchez-Sanchez, M.; C. van Veen, A.; Lercher, J. On the Impact of co-Feeding Aromatics and Olefins for the Methanol-to-Olefins Reaction on HZSM-5. *J. Catal.*, **2014**, *314*, 21−31.
(49) Teketel, S.; Svelle, S.; Lillerud, K.-P.; Olsbye, U. Shape-Selective Conversion of Methanol to Hydrocarbons Over 10-Ring Unidirectional-Channel Acidic H-ZSM-22. *ChemCatChem*, **2009**, *1*, 78−81.
(50) Teketel, S.; Skistad, W.; Benard, S.; Olsbye, U.; Lillerud, K.-P.; Beato, P.; Svelle, S. Shape Selectivity in the Conversion of Methanol to Hydrocarbons: The Catalytic Performance of One-Dimensional 10-ring Zeolites: ZSM-22, ZSM-23, ZSM-48, and EU-1. *ACS Catal.*, **2012**, *2*, 26−37.

Selectively Introducing Acid Sites in Different Confined Positions in ZSM-5 and its Catalytic Implications

Chengeng Li,[†] Alejandro Vidal-Moya,[†] Pablo J. Miguel,[§] Jiri Dedecek,[‡] Mercedes Boronat[†,*] and Avelino Corma[†, *]

[†]Instituto de Tecnología Química, Universitat Politècnica de València, Consejo Superior de Investigaciones Cientificas, Av. de los Naranjos, s/n, 46022 Valencia, Spain

[§]Departamento de Ingeniería Química, Universitat de València, Av. de la Universitat, s/n, 46100 Burjassot, Spain

[‡]J. Heyrovsky Institute of Physical Chemistry, Academy of Sciences of the Czech Republic, Dolejskova 3, CZ-182 23 Prague 8, Czech Republic

Insert Table of Contents artwork here